IEEE Open Journal of
Antennas and Propagation

Received 16 June 2020; revised 12 July 2020; accepted 13 July 2020. Date of publication 17 July 2020; date of current version 10 August 2020.
Digital Object Identifier 10.1109/OJAP.2020.3010153

Mutual Coupling Suppression in Antenna Arrays Using Meandered Open Stub Filtering Technique

SANDHIYA REDDY GOVINDARAJULU [1] (Graduate Student Member, IEEE), ALEXANDER JENKEL [2], RIMON HOKAYEM [1] (Graduate Student Member, IEEE), AND ELIAS A. ALWAN [1] (Member, IEEE)

[1] Electrical and Computer Engineering Department, Florida International University, Miami, FL 33174, USA
[2] College of Engineering and Computer Science, University of Central Florida, Orlando, FL 32816, USA
CORRESPONDING AUTHOR: S. R. GOVINDARAJULU (e-mail: sredd015@fiu.edu)
This work was supported by the National Science Foundation under Award 1943040.

ABSTRACT Multiple-input and multiple-output (MIMO) systems utilize multiple antenna elements to improve channel capacity and achieve higher data rates. The successful implementation of MIMO systems requires low mutual coupling between antenna elements to reduce the envelope correlation coefficient (ECC) at the operating frequency. In this paper, we introduce a mutual coupling suppression technique using an open stub meandered (OSM) bandstop filter (BSF) design for MIMO applications. The OSM-BSF is optimized and implemented on the ground plane side of a two-element patch array. The designed filter provides high isolation of 60 dB at 2.4 GHz across a 30% bandwidth. A parametric study of antenna element spacing was carried out, showing at least 40 dB of mutual coupling suppression in the antenna array, irrespective of the antenna element spacing. A two-element antenna array prototype with OSM-BSF was fabricated and tested. Measurements showed that $\geq$ 57 dB isolation was achieved using OSM-BSF. Besides, the fabricated array provides a low ECC of 0.0093 at 2.42 GHz, while maintaining edge-to-edge spacing as little as $0.19\lambda_0$.

INDEX TERMS Antenna arrays, envelope correlation coefficient (ECC), isolation, mutual coupling, open stub meandered bandstop filter (OSM-BSF).

I. INTRODUCTION

Multiple-input and multiple-output (MIMO) systems employ multiple transmitter and receiver antennas to create many independent communication channels. MIMO takes advantage of multipath propagation to transmit the information effectively and improve radio link capacity [1]–[2]. However, the full benefit of MIMO systems can only be realized by minimizing the coupling between the channels, viz., antennas. In other words, high isolation between antenna elements ensures independent transmission/reception of simultaneous data streams.

The mutual coupling among channels is often characterized by the envelope correlation coefficient (ECC), commonly used in a multi-antenna system. Thus, high isolation between the antennas implies a low ECC. The latter can be improved using different techniques, namely radiation pattern diversity [3]–[4], polarization diversity [5], and port-to-port isolation techniques [6]–[19].

A frequency selective surfaces (FSS)-based correlation technique has been implemented in [3] using radiation pattern diversity. This technique demonstrated an ECC of 0.0022 and an isolation improvement of about 8 dB. In [5], polarization diversity was realized by a progressive angular separation between the antennas. Neighboring elements were rotated by a certain angle with respect to one another. Measured results of a 3×3 MIMO configuration showed diversity gain without requiring any spatial separation.

A combination of pattern and polarization diversity is achieved with a multimode diversity method. The latter uses only one antenna for establishing diversity. That is, the compactness of such systems is achieved by one element with independently fed modes [6]–[10]. Popular port-to-port suppression techniques have been implemented using various structures such as electromagnetic band gap (EBG) [11], defected ground plane (DGS) [11]–[13], complementary split ring resonator (CSRR) [14], and fractals [15]. In [11], a

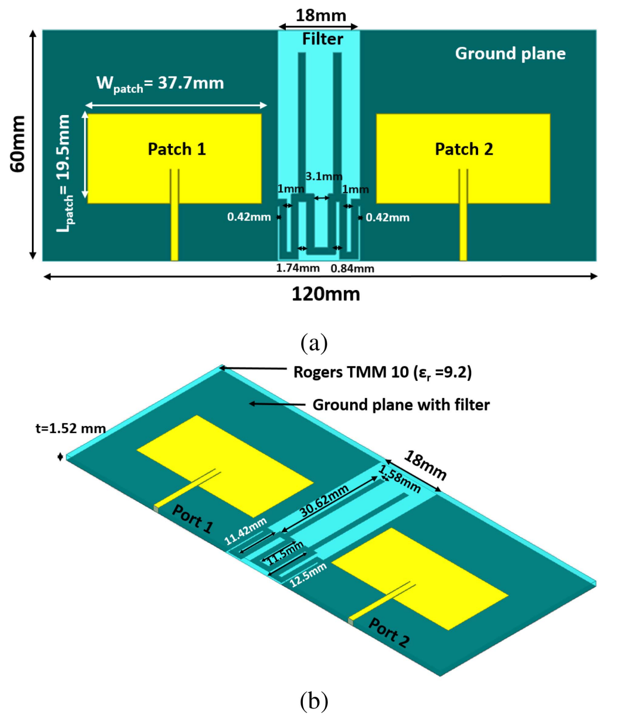

FIGURE 1. Two-element patch array using open stub bandstop filter in the ground plane (a) Top view (b) 3D view.

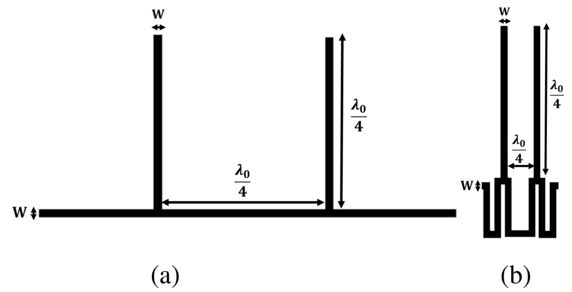

FIGURE 2. (a) Conventional open stub bandstop filter (b) Meandered open stub bandstop filter.

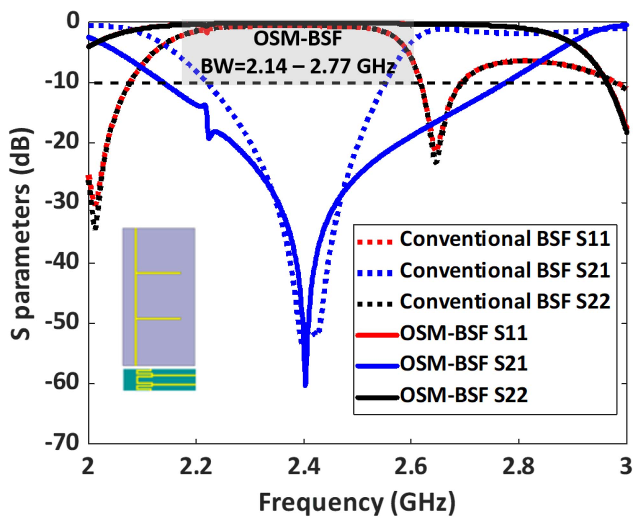

FIGURE 3. Simulated S-parameters of the conventional BSF and OSM bandstop filter.

patch antenna with both EBG and DGS structures was implemented, showing port isolation improvement of a maximum of 22 dB across the operating bandwidth. A double-layer mushroom structure, presented in [16], provided a port isolation improvement of 42 dB and an ECC < 0.02 across the operating bandwidth. However, the addition of vias limits this technique.

Decoupling using slotted-CSRR was also implemented for MIMO arrays in [14]. Nevertheless, this technique only provided 10 dB improvement in isolation. In [17], the insertion of complementary meandered slot lines on the ground plane leads to isolation of 34.3 dB. However, the fabrication of these micromachined slots involves complicated processes such as ultra-violet (UV) lithography and electroplating. In [18], a metasurface superstrate was implemented to suppress the mutual coupling, providing an isolation enhancement of 40 dB. Other works included fractal loads [15] showing 37 dB of isolation improvement. Similarly, a decoupling network was employed in [19] to achieve an additional mutual coupling suppression of 20 dB.

In this paper, a mutual coupling suppression technique with port-to-port isolation is presented using an open stub meandered bandstop filter for MIMO applications. As shown in Fig. 1(a), the bandstop filter is composed of two quarter-wavelength stubs connected with a meandered transmission line, implemented on the ground plane side between antenna elements. This filter provides high port-to-port isolation of 60 dB at the operating frequency. Our design is particularly optimized with a two-element array, as depicted in Fig. 1(b). The filter acts as a barrier at the operating frequency and absorbs the near fields between the antenna elements, thus significantly improves the port-to-port isolation. A prototype was fabricated, tested, and measured. The experimental results show high isolation of 57 dB while maintaining an ECC less than 0.03 in the operating bandwidth (viz., 2.4-2.43 GHz) with low ECC of 0.0093 at 2.42 GHz. Our simple single-layer 1×2 array design provides a realized gain of 6.95 dBi with a center-to-center spacing of $0.5\lambda_0$ (edge-to-edge spacing of $0.19\lambda_0$).

The paper is organized as follows: in Section II, the principle and characteristics of the open stub meandered bandstop filter with its equivalent circuit are described. The array design with integrated filter and parametric studies are then presented in Section III. Finally, Section IV describes the fabrication details and measurements, and Section V concludes the paper.

II. MUTUAL COUPLING SUPPRESSION TECHNIQUE

A conventional open stub bandstop filter (BSF) that consists of two quarter-wavelength ($\lambda_0/4$) open stubs placed $\lambda_0/4$ apart, where λ_0 is the freespace wavelength of the microstrip line at the center frequency, is shown in Fig. 2(a). The quarter wavelength stubs are placed in shunt along the transmission line to provide bandstop filter characteristics.

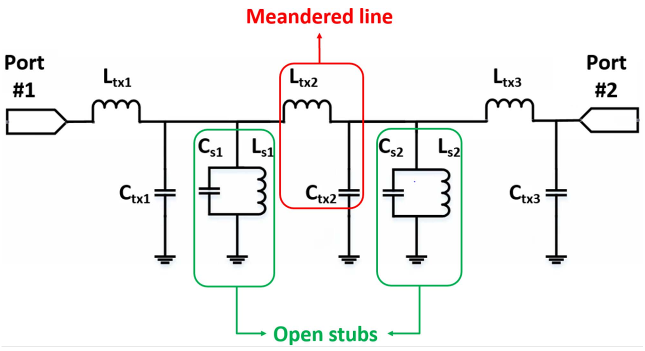

FIGURE 4. Equivalent circuit of the OSM-BSF.

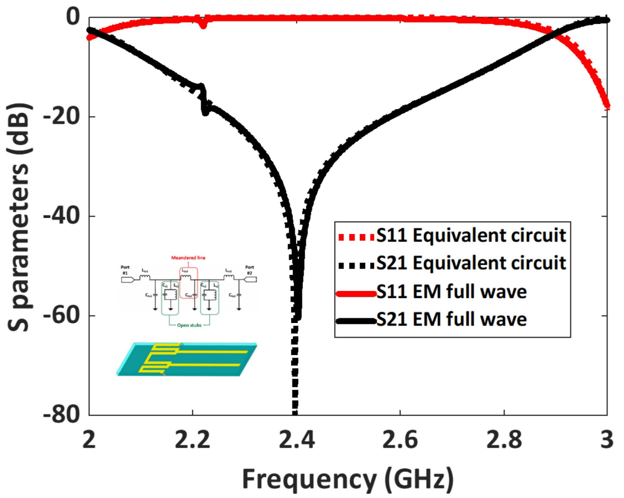

FIGURE 5. S-parameters comparison between full-wave and equivalent circuit simulators of the designed OSM-BSF.

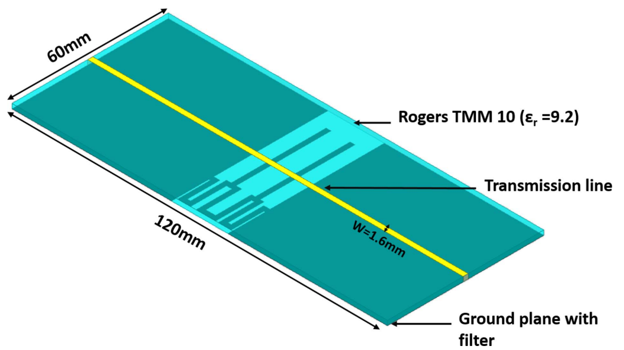

FIGURE 6. 3D view of the 50Ω transmission line with a filter in the ground plane.

We note that additional stubs can be included to improve rejection and achieve a wider stopband [20]. However, these stubs increase the physical dimension of the filter, making it unsuitable for low profile antenna arrays. To reduce the overall filter's circuit size and achieve higher rejection, an open stub meandered BSF (OSM-BSF) is presented in this paper, as depicted in Fig. 2(b). The filter is simple and easy to fabricate on a low cost in-house printed circuit board (PCB).

To evaluate the filter's performance, a conventional BSF and an OSM-BSF are designed on a TMM10 substrate with

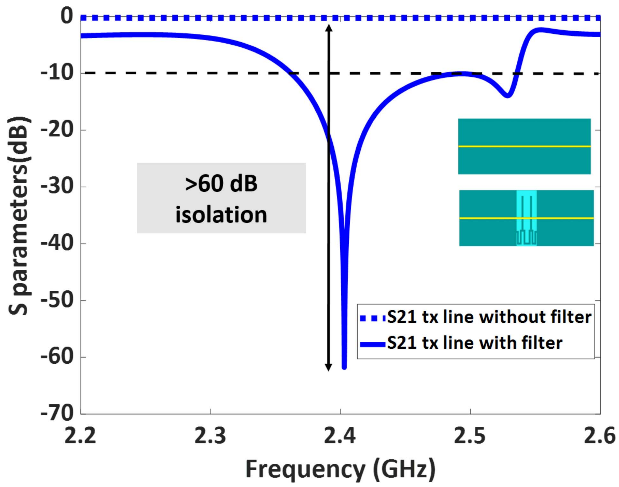

FIGURE 7. Simulated S_{21}(dB) of the transmission line with and without OSM-BSF.

TABLE 1. Optimized values of the OSM-Band stop filter.

C_{tx1}	3.9 nH
L_{tx1}	3 pF
C_{s1}	5.8 nH
L_{s1}	0.76 pF
C_{tx2}	2.1 nH
L_{tx2}	25.5 pF
C_{s2}	0.25 nH
L_{s2}	100 pF
C_{tx3}	0.6 nH
L_{tx3}	6.5 pF

a dielectric constant $\epsilon_r = 9.2$, a thickness of 1.52 mm, and a dielectric loss tangent $tan\delta = 0.0022$. As depicted in Fig. 3, simulations show that the OSM-BSF provides a high isolation of 60 dB at 2.4 GHz with a bandwidth of 2.14-2.77 GHz. Notably, the dimensions of the conventional BSF are 150 mm × 60 mm×1.52 mm, and the dimensions of the OSM-BSF are 18 mm× 60 mm× 1.52 mm. As such, the OSM-BSF offers 84% reduction in size as compared to conventional BSF. Fig. 4 depicts the equivalent circuit model of the OSM-BSF. The meandered lines are represented using inductance L_{tx} and capacitance C_{tx} [23]. The resonant frequency of open stubs depends upon the stub inductance L_s and the stub capacitance C_s, such as,

$$f_c = \frac{1}{2\pi\sqrt{L_s C_s}} \quad (1)$$

The equivalent circuit model was optimized using a circuit simulator to match the full-wave simulations. The inductance and capacitance values of the equivalent circuit are displayed in Table 1. Fig. 5 shows excellent agreement between the S-parameters of the full-wave and equivalent circuit simulators.

Next, the effect of placing the OSM bandstop filter on the ground plane is investigated using a 50Ω transmission line operating at 2.4 GHz, as shown in Fig. 6. The dimensions of the transmission line are 120 mm× 1.6 mm × 1.52 mm. The same transmission line was also simulated without the addition of the OSM-BSF for comparison. Results show that the

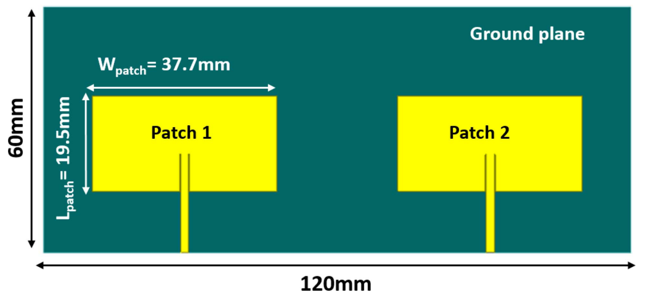

FIGURE 8. A two-element reference patch array without OSM-BSF.

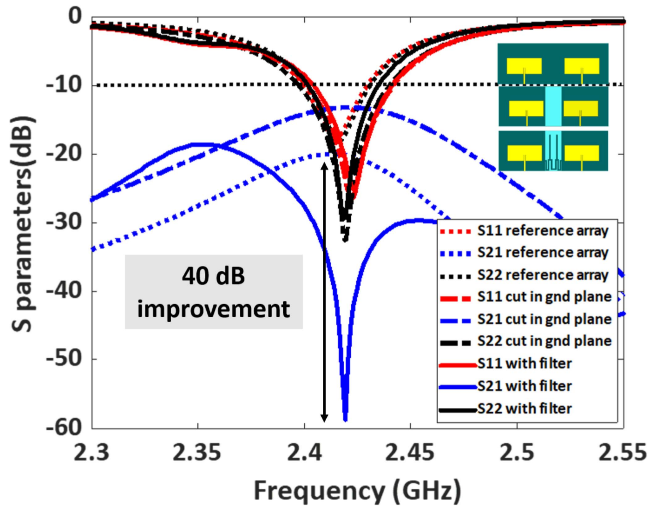

FIGURE 9. Comparison between the simulated antenna array with and without open stub meandered bandstop filter.

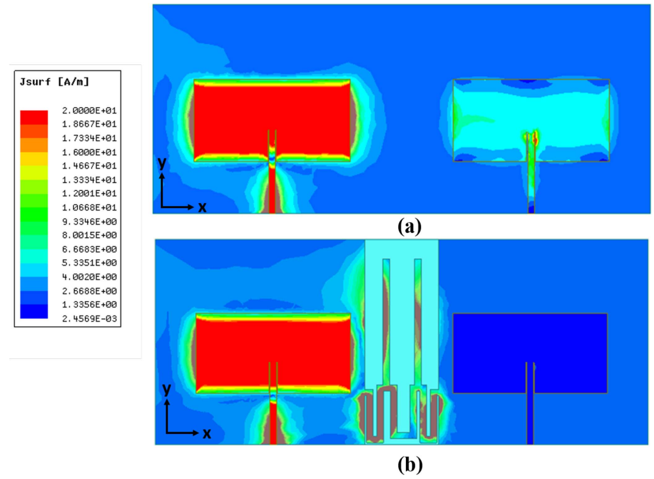

FIGURE 10. Current distribution over the surfaces of the patch antenna array (a) without filter (b) with filter.

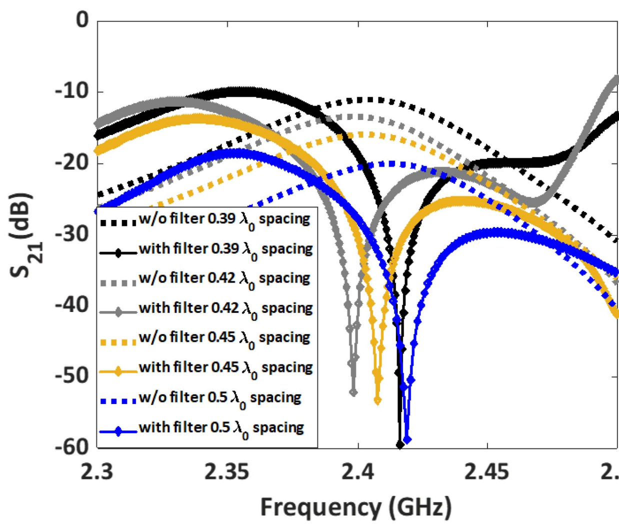

FIGURE 11. S_{21} (dB) with and without filter at different antenna element spacing.

addition of the OSM-BSF to the transmission line's ground plane provides an isolation >60 dB between the ports, as depicted in Fig. 7. As such, high port-to-port isolation is achieved by inserting our OSM-BSF on the ground plane.

III. DESIGN PROCESS

A. ANTENNA DESIGN

To evaluate this mutual coupling technique for MIMO applications, we designed a two-element patch array on a Rogers TMM 10 substrate. For reference, the patched array is first designed without OSM-BSF, as depicted in Fig. 8. The patch elements are placed at a distance $\lambda_0/2$ apart, with overall dimensions of 120 mm × 60 mm × 1.52 mm (viz., $0.96\lambda_0 \times 0.48\lambda_0 \times 0.012\lambda_0$).

The simulated antenna array is perfectly matched to a 50Ω port impedance at 2.42 GHz and provides a −10 dB impedance bandwidth across 2.4-2.43 GHz (see Fig. 9). Results showed that the reference patch array (viz., without OSM-BSF) exhibited a high mutual coupling across the operating bandwidth, implying that the fields of each antenna are strongly coupled with one another, as illustrated in Fig. 10 (a). Clearly, without OSM-BSF, a high concentration of the surface currents is observed in the terminated antenna.

The isolation between antenna elements pairs is enhanced by placing the OSM-BSF on the ground plane, as depicted in Fig. 1. Particularly, the OSM-BSF operates at 2.42 GHz and is optimized to suppress the surface currents in the ground plane. To further investigate the surface current distributions of the array with OSM-BSF, we excited one of the patches and terminated the other with a 50Ω load impedance. In this case, Fig. 10(b) clearly shows that the addition of an OSM bandstop filter in the ground plane between the antenna elements mitigated the surface currents. As a result, the coupling between antenna elements drastically reduced by >40dB, as clearly illustrated in Fig. 9. To validate that the isolation improvement is only due to the addition of the filter, we introduced a cut in the ground plane without the filter and computed the S-parameters, as also shown in Fig. 9. The S_{21} plot in this case shows that the coupling is as high as 15dB, which clearly indicates that the addition of the OSM-BSF on the ground plane is improving the isolation between the patches. Notably, the array maintained a low profile with an edge-to-edge spacing of $0.19\lambda_0$.

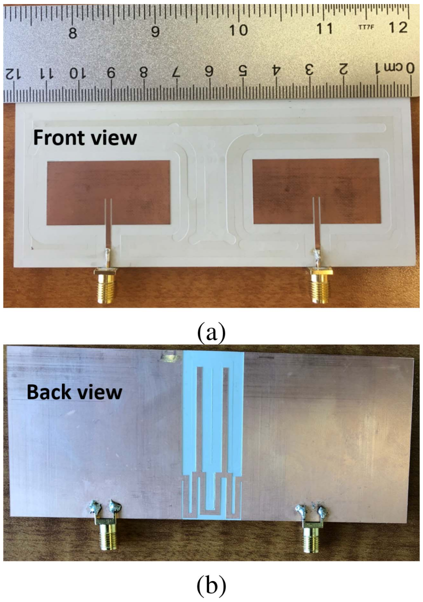

FIGURE 12. Fabricated 2 element antenna array (a) top view (b) bottom view.

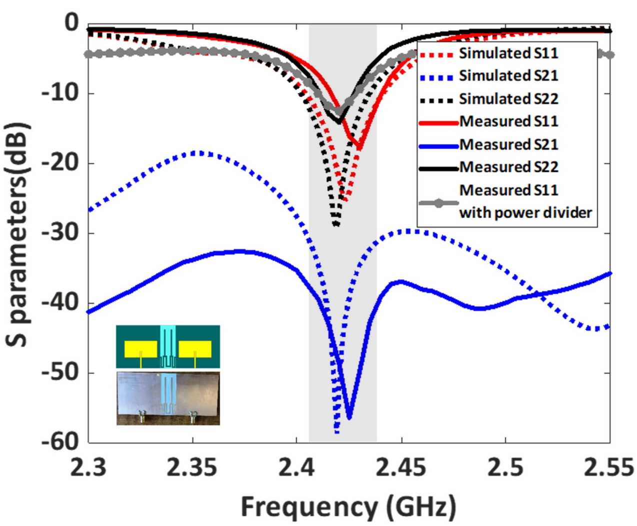

FIGURE 13. Simulated and measured S-parameters of the two-element antenna array using OSM-BSF with and without power divider.

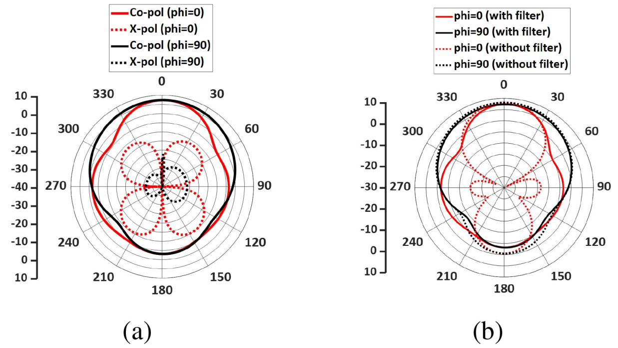

FIGURE 14. Simulated radiation pattern (dB) of the array (a) co-polarization and cross-polarization of the array (b) Pattern with and without filter in the ground plane.

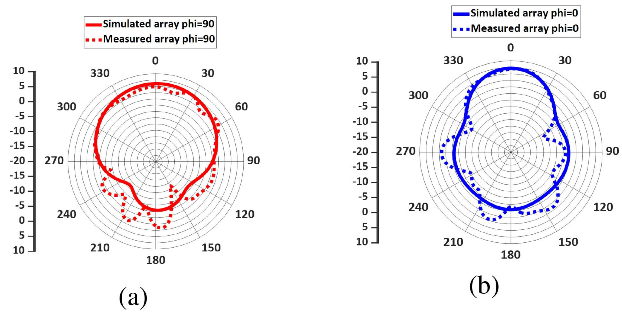

FIGURE 15. Measured and simulated radiation pattern (dB) of the array (a) phi = 90 (E plane) (b) phi = 0 (H plane).

B. PARAMETRIC STUDIES

To analyze the effect of OSM-BSF with different antenna element spacing, a parametric study was conducted. By varying the array's center-to-center spacing from $0.39\lambda_0$ to $0.5\lambda_0$ and the parameters such as length of the stubs, the length of the meandered line, the position of the filter on the ground plane were optimized. From Fig. 11, it is evident that the implemented technique is capable of generating almost 40 dB isolation improvement, irrespective of the antenna element spacing. Particularly, when the center-to-center spacing is maintained at $0.39\lambda_0$ a high isolation enhancement of about 48dB is achieved. This indicates that the OSM-BSF technique is potential great candidate for closely spaced MIMO antennas.

IV. MEASUREMENT RESULTS

A. S-PARAMETERS AND RADIATION PATTERN

The 1×2 patch antenna array with OSM-BSF was fabricated and tested. For our prototype, we choose center-to-center spacing $0.5\lambda_0$. Fig. 12 shows the top and back view of the fabricated prototype. Measured S-parameters with and without power divider are illustrated in Fig. 13. As expected, the 1×2 patch antenna array is well-matched to 50Ω (viz., $S_{11} < -10$ dB) at both ports across 2.4-2.43 GHz. Importantly, the measured mutual coupling was >57dB at 2.42 GHz, which corresponds to 37dB improvement from the reference design (see Fig. 9). As such, the bandstop filter on the ground plane acted as a barrier at the operating frequency. The slight frequency shift between the simulated and measured results is due to fabrication tolerances and measurement errors. The radiation patterns in the E and H planes are computed by exciting the two antennas using a power divider. The array with OSM-BSF exhibited low cross-polarization levels in both E and H planes, as illustrated in Fig. 14 (a). To study the effect of filter on the radiation pattern, simulations were conducted for the array with and without the OSM-BSF filter. As depicted in Fig. 14(b), the addition of the filter does not affect the gain of the array. Further, the radiation pattern in the E-plane remains the same after adding the filter. In the H-plane, the patterns agree well from $+45^0$ to -45^0. The slight variation of the radiation pattern for larger angles can be circumvented by connecting the gap between the two ground planes. Further, the simulated

TABLE 2. Comparison between the implemented technique and the other methods.

References	Technique	Resonant frequency (BW)	Dimensions of the array	Center-to-center spacing	Edge-to-edge spacing	Diversity	ECC	Maximum isolation improvement
[3]	FSS	5.25GHz (5.15-5.3GHz)	$1.83\lambda_0 \times 0.83\lambda_0 \times 0.25\lambda_0$	$0.52\lambda_0$	$0.13\lambda_0$	Radiation pattern	0.0022	8 dB
[11]	EBG+DGS	4.82-5GHz	$0.88\lambda_0 \times 0.44\lambda_0 \times 0.02\lambda_0$	$0.36\lambda_0$	$0.13\lambda_0$	Radiation pattern	<0.002	22 dB
[13]	Resonant slot	5.8GHz (5.75-5.85GHz)	$0.85\lambda_0 \times 0.55\lambda_0$	$0.33\lambda_0$	$0.031\lambda_0$	Port-port isolation	NA	40 dB
[15]	Fractal load	Multi-band 8.7-34.2 GHz	23mm×23mm×1.6mm	$1.39\lambda_0$	$0.65\lambda_0$	Port-port isolation	NA	37 dB
[17]	Meandered line slots	4.94-4.99 GHz	70mm×50mm×1.52mm ($1.14\lambda_0 \times 0.81\lambda_0 \times 0.024\lambda_0$)	$0.25\lambda_0$	$0.032\lambda_0$	Port-port isolation	NA	11(min.)-34.3 dB(max.)
[19]	Decoupling network	2.4GHz (2.4-2.5GHz) and 5.2GHz (5.15-5.35 GHz)	$1.4\lambda_0 \times 0.96\lambda_0 \times 0.028\lambda_0$	$0.22\lambda_0$	$0.17\lambda_0$	Port-port isolation	0.13 (2.4GHz) 0.008 (5.25GHz)	20 dB
[22]	Compact EBG	2.4GHz (2.4-2.8GHz)	84mm×18.2mm	$0.8\lambda_0$	$0.47\lambda_0$	Port-port isolation	NA	17 dB
This work	**Open stub bandstop filter**	**2.42GHz (2.4-2.43 GHz)**	**120mm×60mm×1.52mm ($0.96\lambda_0 \times 0.48\lambda_0 \times 0.012\lambda_0$)**	**$0.39\lambda_0$-$0.5\lambda_0$**	**$0.089\lambda_0$-$0.19\lambda_0$**	**Port-port isolation**	**0.0093**	**48-40 dB(sim.) 37 dB (meas.)**

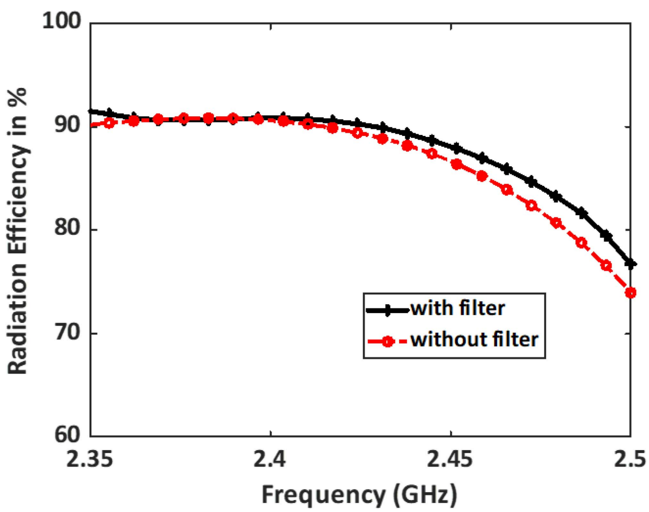

FIGURE 16. Radiation efficiency of the two-element array with and without filter.

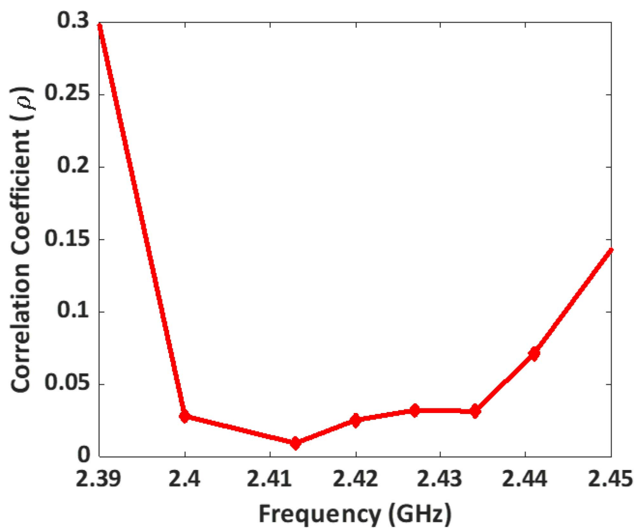

FIGURE 17. The calculated envelope correlation coefficient of the array using far-field patterns.

and measured radiation patterns are in good agreement (see Fig. 15 (a) and (b)). Also, the realized gain was measured to be 6.95 dBi in both E and H planes. Fig. 16 shows the simulated radiation efficiency of the array with and without filter. It is clear that the radiation efficiency with filter is approximately 90% across the operating band.

B. MIMO CORRELATION COEFFICIENT

The spectral efficiency of the communication channel can be enhanced by reducing the mutual coupling and improving isolation between antenna elements in MIMO systems. This mutual coupling is often characterized by the ECC denoted ρ_{ij}, and computed using far-field radiation patterns, as follows [24],

$$\rho_{ij} = \frac{\left|\int\int F_i(\theta,\phi) * F_j(\theta,\phi) d\Omega\right|^2}{\int\int |F_i(\theta,\phi)|^2 d\Omega \int\int \left|F_j(\theta,\phi)\right|^2 d\Omega} \tag{2}$$

where $F_i(\theta,\phi)$ is the complex field pattern radiated from the i^{th} element. Using (2), ρ_{ij} was computed for a two element array at different frequencies points from 2.39 GHz to 2.45 GHz, as shown in Fig. 17. The ECC remains lower than

0.03 within the operating bandwidth (2.4-2.43 GHz) with a low ECC of 0.0093 at the center frequency, viz., 2.42 GHz.

In Table 2, our array with OSM-BSF is compared against various techniques used in MIMO systems. Clearly, our design provides higher isolation and low correlation coefficient as compared to the other methods while maintaining a low-profile feature (edge-to-edge spacing $0.19\lambda_0$).

V. CONCLUSION

In this paper, we presented a new coupling reduction technique for MIMO applications using an open stub meandered bandstop filter on the ground plane. Our OSM-BSF demonstrated 1) about 40 dB isolation improvement between the array elements and 2) a low envelope correlation coefficient of 0.0093. Additionally, parametric analysis indicates that this technique is even applicable to closely spaced antennas with edge-to-edge spacing up to $0.089\lambda_0$. A prototype with a two-element patch antenna was fabricated and tested for validation. Importantly, our OSM-BSF is compact and easy to implement. Overall, this technique provides avenues for a new class of mutual coupling suppression techniques where high isolation plays a crucial factor in defining the system's performance.

REFERENCES

[1] T. L. Marzetta and B. M. Hochwald, "Capacity of mobile multiple antenna communication link in Rayleigh flat fading," *IEEE Trans. Inf. Theory*, vol. 45, no. 1, pp. 139–157, Jan. 1999.

[2] I. E. Telatar, "Capacity of multi-antenna Gaussian channels," AT&T Bell Lab., Atlanta, GA, USA, Rep. BL0112170-950615-07TM, 1995.

[3] T. Hassan, M. U. Khan, H. Attia, and M. S. Sharawi, "An FSS based correlation reduction technique for MIMO antennas," *IEEE Trans. Antennas and Propag.*, vol. 66, no. 9, pp. 4900–4905, Sep. 2018.

[4] M. Akbari, M. M. Ali, M. Farahani, A. R. Sebak, and T. Denidni, "Spatially mutual coupling reduction between CP-MIMO antennas using FSS superstrate," *Electron. Lett.*, vol. 53, no. 8, pp. 516–518, Apr. 2017.

[5] J. F. Valenzuela-valdes, M. A. Garcia-fernandez, A. M. Martinez-gonzalez, and D. Sanchez-Hernandez, "The role of polarization diversity for MIMO systems under Rayleigh-fading environments," *IEEE Antennas Wireless Propag. Lett.*, vol. 5, pp. 534–536, 2006.

[6] C. Waldschmidt and W. Wiesbeck, "Compact wide-band multimode antennas for MIMO and diversity," *IEEE Trans. Antennas Propag.*, vol. 52, no. 8, pp. 1963–1969, Aug. 2004.

[7] T. Svantesson, "Correlation and channel capacity of MIMO systems employing multimode antennas," *IEEE Trans. Veh. Technol.*, vol. 51, no. 6, pp. 1304–1312, Nov. 2002.

[8] E. N. Gilbert, "Energy reception for mobile radio," *Bell Syst. Techn. J.*, vol. 44, no. 8, pp. 1779–1803, Oct. 1965.

[9] R. G. Vaughan and J. B. Andersen, "A multiport patch antenna for mobile communications," in *Proc. 14th Eur. Microw. Conf.*, Liege, Belgium, 1984, pp. 607–612.

[10] T. Svantesson, "An antenna solution for mimo channels: The multimode antenna," in *Proc. Conf. Rec. 34th Asilomar Conf. Signals Syst. Comput.*, vol. 2. Pacific Grove, CA, USA, 2000, pp. 1617–1621.

[11] Y. Liu, X. Yang, Y. Jia, and Y. J. Guo, "A low correlation and mutual coupling MIMO antenna," *IEEE Access*, vol. 7, pp. 127384–127392, 2019.

[12] A. Habashi, J. Nourinia, and C. Ghobadi, "A rectangular defected ground structure (DGS) for reduction of mutual coupling between closely-spaced microstrip antennas," in *Proc. 20th Iran. Conf. Elect. Eng. (ICEE)*, Tehran, Iran, 2012, pp. 1347–1350.

[13] J. OuYang, F. Yang, and Z. M. Wang, "Reducing mutual coupling of closely spaced microstrip MIMO antennas for WLAN application," *IEEE Antennas Wireless Propag. Lett.*, vol. 10, pp. 310–313, 2011.

[14] M. M. Bait-Suwailam, O. F. Siddiqui, and O. M. Ramahi, "Mutual coupling reduction between microstrip patch antennas using slotted-complementary split-ring resonators," *IEEE Antennas Wireless Propag. Lett.*, vol. 9, pp. 876–878, 2010.

[15] M. Alibakhshikenari, M. Khalily, B. S. Virdee, C. H. See, R. A. Abd-Alhameed, and E. Limiti, "Mutual coupling suppression between two closely placed microstrip patches using EM-bandgap metamaterial fractal loading," *IEEE Access*. vol. 7, pp. 23606–23614, 2019.

[16] G. Zhai, Z. N. Chen, and X. Qing, "Enhanced isolation of a closely spaced four-element MIMO antenna system using metamaterial mushroom," *IEEE Trans. Antennas Propag.*, vol. 63, no. 8, pp. 3362–3370, Aug. 2015.

[17] S. Hwangbo, H. Y. Yang, and Y. Yoon, "Mutual coupling reduction using micromachined complementary meander-line slots for a patch array antenna," *IEEE Antennas Wireless Propag. Lett.*, vol. 16, pp. 1667–1670, 2017.

[18] H. Luan, C. Chen, W. Chen, L. Zhou, H. Zhang, and Z. Zhang, "Mutual coupling reduction of closely E/H-plane coupled antennas through metasurfaces," *IEEE Antennas Wireless Propag. Lett.*, vol. 18, pp. 1996–2000, 2019.

[19] L. Zhao and K. Wu, "A dual-band coupled resonator decoupling network for two coupled antennas," *IEEE Trans. Antennas Propag.*, vol. 63, no. 7, pp. 2843–2850, Jul. 2015.

[20] W.-H. Tu and K. Chang, "Compact microstrip bandstop filter using open stub and spurline," *IEEE Microw. Wireless Comp. Lett.*, vol. 15, no. 4, pp. 268–270, Apr. 2005.

[21] S. Blanch, J. Romeu, and I. Corbella, "Exact representation of antenna system diversity performance from input parameter description," *Electron. Lett.*, vol. 39, no. 9, pp. 705–707, May 2003.

[22] M. T. Islam and M. S. Alam, "Compact EBG structure for alleviating mutual coupling between patch antenna array elements," *Progr. Electromagn. Res.*, vol. 137, pp. 425–438, 2013, doi: 10.2528/PIER12121205.

[23] R. Sato, "A design method for meander-line networks using equivalent circuit transformations," *IEEE Trans. Microw. Theory Techn.*, vol. 19, no. 5, pp. 431–442, May 1971.

[24] R. G. Vaughan and J. B. Andersen, "Antenna diversity in mobile communications," *IEEE Trans. Veh. Technol.*, vol. 36, no. 4, pp. 149–172, Nov. 1987.

[25] A. Iqbal, O. A. Saraereh, A. W. Ahmad, and S. Bashir, "Mutual coupling reduction using *F*-shaped stubs in UWB-MIMO antenna," *IEEE Access*, vol. 6, pp. 2755–2759, 2017.

[26] A. A. Chaudhari and R. K. Gupta, "A simple tri-band MIMO antenna using a single ground stub," *Progr. Electromagn. Res.* vol. 86, pp. 191–201, 2018, doi: 10.2528/PIERC18061803.

SANDHIYA REDDY GOVINDARAJULU (Graduate Student Member, IEEE) received the B.E. degree in electronics and communication engineering and the M.E. degree in communication systems from Anna University, Chennai, India, in 2013 and 2015, respectively. She is currently pursuing the Ph.D. degree with Florida International University, Miami, FL, USA.

She was an Intern Researcher with the Society for Applied Microwave Electronics Engineering and Research, India, during her master's degree studies. She was a Program Analyst with Cognizant Technology Solutions, Chennai, India. Her research interests include millimeter-wave antennas for 5G communication systems, beamforming, and RF front end.

Ms. Govindarajulu received the Best Student Paper Award for her research work at iWAT 2019.

ALEXANDER JENKEL was born in October 1996. He received the Bachelors of Science degree in electrical engineering from the University of Central Florida, Orlando, FL, USA, in 2020.

He began his engineering career doing research over the summer of 2019 with Florida International University, Miami, FL, USA, with Dr. Elias Alwan's RF Communications Lab. Following a successful summer program, he began to do research with Dr. Zhishan Guo's Real Time Systems Lab, University of Central Florida.

RIMON HOKAYEM (Graduate Student Member, IEEE) received the master's degree in telecommunications engineering from the Lebanese University Faculty of Engineering in 2014. He is currently pursuing the Ph.D. degree in electrical engineering with the Department of Electrical and Computer Engineering, Florida International University, Miami, FL, USA. He completed his master's project during his internship with the Centre de Sciences Nucléaires et de Sciences de la Matière (CSNSM/IN2P3/CNRS), Ile-de-France, France. His thesis focuses on field-programable gate array programming for data acquisition and processing of gamma-rays. Since 2014, he has been working as a Software Engineer. His research interests focus on radio frequency systems with an emphasis on millimeter-wave communications, beamforming, and reduction in hardware, and power consumption.

ELIAS A. ALWAN (Member, IEEE) was born in Aitou, Lebanon, in 1984. He received the B.E. degree (*summa cum laude*) in computer and communication engineering from Notre Dame University–Louaize, Zouk Mosbeh, Lebanon, in 2007, the M.E. degree in electrical engineering from the American University of Beirut, Beirut, Lebanon, in 2009, and the Ph.D. degree in electrical and computer engineering from Ohio State University (OSU), Columbus, OH, USA, in 2014. He is an Assistant Professor with the Electrical and Computer Engineering Department, Florida International University. He was a Senior Research Associate with the ElectroScience Laboratory, OSU, from 2015 to 2017. His research is in the areas of antennas and radio frequency systems with particular focus on ultra-wideband communication systems, including UWB arrays, reduced hardware and power-efficient communication back-ends, and millimeter-wave technologies for 5G applications. He is the recipient of the 2020 NSF CAREER Award. He has been a Phi Kappa Phi Member since 2010.